Article

Not peer-reviewed version

Method for Determining Stresses in the Soil Layer Under the Action of a Dihedral Wedge

Anton Kuvaev *, Alexey Derepaskin, Ivan Tokarev, Yurij Binyukov, Yurij Polichshuk, Pavel Ivanchenko, Alexander Semibalamut

Posted Date: 11 May 2026

doi: 10.20944/preprints202605.0665.v1

Keywords: dihedral wedge; stress distribution; soil deformation; graphical–analytical method; Boussinesq equation

 doi:10.20944/preprints202605.0665.v1

Article

Method for Determining Stresses in the Soil Layer Under the Action of a Dihedral Wedge

Anton Kuvaev *, Alexey Derepaskin, Ivan Tokarev, Yurij Binyukov, Yurij Polichshuk, Pavel Ivanchenko and Alexander Semibalamut

Kostanay branch of «Scientific production center of agricultural engineering», LLP, Abay Ave., 34, 110000 Kostanay, Republic of Kazakhstan

* Correspondence: e-mail: kuvaevanthon@yandex.ru

Abstract

The experimental determination of the relationships between the stress distribution zone in the soil layer and the parameters of tillage working bodies is a labor-intensive process. Therefore, preliminary mathematical modeling of this process is recommended to minimize the total number of experiments. The research was conducted using the principles of classical mechanics and soil mechanics. Using an equation proposed by J. Boussinesq,a graphical-analytical method was developed to evaluate the stress state in the soil layer induced by a dihedral wedge. This method incorporates both the geometric parameters of the dihedral wedge and the physico-mechanical properties of the soil. A direct proportional relationshipwas established between the length of the dihedral wedge and the total area of the deformed soil mass. Specifically, increasing the length of the dihedral wedge by 83% (from 0.05 to 0.30 m) resulted in an 80% increase in the area of the deformed soil mass (from 0.02 to 0.10 m²). The proposed graphical–analytical method can be employed in the design of tillage implements.

Keywords: dihedral wedge; stress distribution; soil deformation; graphical–analytical method; Boussinesq equation

1. Introduction

Soil compaction, a consequence of various anthropogenic factors, represents a significant challenge in contemporary agricultural production [1].

The management of soil compaction is carried out in three directions[2–6]: reduction of compaction, prevention of compaction, and decompaction.

To reduce soil compaction, several measures have been proposed. These include improvementsin propulsion systems of power units (dual wheels, low-pressure tyres, rubber-metal tracks), reduction of their weight, creation of wide-span and combined machines, and routing of the movement of machine-tractor units (technological wheel tracks) [7–9].

It is evident that the measures currently in place to prevent soil compaction are insufficient and require further development and study. This field of work may encompass machines operating on an air cushion, as well as the concept of bridge farming [10–13]. However, implementing such technologies will require significant capital investment for long-term research and development. In this regard, at the current stage of scientific and technological development, the most effective method for combating soil compaction is its decompaction.

Methods of artificial or technical soil decompaction can be classified as follows:

a) mechanical decompaction methods;

b) methods based on hydraulic principles;

c) methods based on the use of gas-air combinations;

d) methods based on gas-dynamic action;

e) methods based on wave (vibratory, electromagnetic) action.

 doi:10.20944/preprints202605.0665.v1

In the current stage of scientific and technological development, deep mechanical tillage is regarded as the most effective method of soil decompaction [14,15].The remaining methods are alternative, whose purpose is, as a rule, to reduce draft resistance [16,17]. Nevertheless, the reduction in draft resistance is counterbalanced by the escalating energy costs neededto operate technical equipmentthat implements hydraulic, gas-dynamic, or other types of impact.

Mechanical tillage can be defined as the mechanical action of tillage implements on the cultivated soil layer. This processprimarily involves the disintegration of the soil monolith into structural aggregates, the rearrangement of these aggregates, and an increase in the volume of air-filled pores between them. The size distribution of soil aggregates and their quantitative proportion are regulated byagronomic requirements. Consequently, under non-moldboard (conservation) tillage, a minimum of 60% of soil aggregates (clods) must have a characteristic dimension of ≤ 5.0 cm [18].

The disintegration of the soil monolith into individual aggregates occurs when the stress developed in a given cross-section of the soil layer due to the action of a working body (deformer) exceeds the soil's strength limit for the predominant type of deformation.

The following classification of working elements is proposed, based on the mechanical method of soil decompaction:

1. By the presence of a drive:
   - traction-driven working elements (with external or active drive);
   - traction working elements (without drive or passive working elements);
2. By the degree of soil layer turnover:
   - with turnover of the cultivated soil layer by more than 135° (moldboard treatment);
   - without turnover of the cultivated soil layer (non-moldboard treatment);
3. By tillage depth:
   - for conventional tillage (16–24 cm);
   - for deep tillage (more than 24 cm);
4. By the ratio of the working element's working width to the width of the directly cultivated field surface:
   - for continuous tillage;
   - for strip tillage;
5. By the type of predominant deformation:
   - compression deformation;
   - tensile deformation;
   - shear deformation;
6. By the trajectory of movement:
   - working elements with translational motion;
   - working elements with rotational motion.

The existing working elements for mechanical soil decompaction are predicated on dihedral and trihedral wedges, as well as their various combinations, and because soil deformation under dihedral and trihedral wedges is identical according to [19], for the sake of convenience, the dihedral wedge will be considered as the soil-deforming element in this study.

The distribution of compressive stresses in soil under the action of a dihedral wedge was investigated by Vagin [20], who experimentally determined the stress distribution zones for different soil types.

In the work [21], the authors reviewed and synthesized the results of experimental studies conducted at different times, in which patterns of stress distribution in the soil layer were identified in both longitudinal and transverse planes using load-measuring sensors buried at various depths, as in the previous example. Furthermore, the impact of the wedge's translational velocity on alterations in the soil layer's strength limit during deformation was investigated.

 doi:10.20944/preprints202605.0665.v1

Such studies maintain their pertinence in the contemporary context, as the effective design of contemporary high-performance machinery capable of efficiently performing technological operations is contingent upon the stage of mathematical and physical modeling of the interaction between the tillage working body and the soil. Consequently, research in this area is being conducted by both domestic [22] and international researchers [23–25].

The results of the aforementioned studies facilitate a comprehensive characterization of the nature and rate of propagation of stresses and deformations in the soil ahead of the wedge.

When the objective of the research is to establish the relationship between the wedge parameters and the zone of ultimate stress distribution that leads to the failure of the soil monolith, conducting such labor-intensive experimental investigations is reasonable only if preliminary theoretical calculations are available, as these can help minimize the total number of experiments. However, the extant works reviewed above [22–25] do not provide methods for performing such calculations.

In work [26], analytical expressions were proposed to determine the extent of stress propagation in the soil under an external load. However, these expressions do not account for the geometric and operational parameters of the soil-deforming element.

A similar mathematical model describing the relationship between the mechanical properties of the soil and the parameters of the deforming element, is presented in [27]. This model considers soil zones where shear and tensile stresses predominate. However, the authors do not address the failure of the soil monolith under compressive stresses, which is the most common scenario during deep tillage of compacted fine-textured soils (loams).

The aim of the research

In this context, the aim of the present study is to develop a graphical–analytical method that, at the stage of theoretical investigations, will make it possible to determine the relationship between the stress distribution zone ahead of a dihedral wedge and its geometric parameters.

2. Materials and Methods

The developed graphical–analytical method is predicated on the principles of classical mechanics and soil mechanics. The research employed a scientific method that included the use of mathematical modeling, abstraction, analysis, and synthesis.

The methodology for conducting experimental research was based on the provisions of the current regulatory documentation, namely: conditions for conducting experimental research — in accordance with GOST 20915 [28], determination of tillage depth — in accordance with GOST 33736 [29], and strain gauging of dihedral wedge variants — in accordance with GOST 34631 [30].

2.1. Methodology for Theoretical Determination of Stresses in the Soil Layer Under the Action of a Dihedral Wedge

Stress values arising at various points within the soil layer due to the action of a wedge were determined using the equation proposed by J. Boussinesq [31]. According to Figure 1, this equation delineates the stress distribution within the soil mass under the influence of a concentrated force P applied at point O:

$$\sigma_R = \frac{3 \cdot P \cdot cos\beta_R}{2 \cdot \pi \cdot R^2}, \quad (1)$$

where σ_R is the stress at the considered point M, Pa;

P is the concentrated force, N;

β_R is the angle between the line of action of force P and the arbitrary point M;

R is the distance from the point of application of the force to the considered point M, m.

By comparing the calculated value of σ_R with the value of $\sigma_{assum.compr}$ it is possible to infer the nature of the impact (failure or partial deformation) of the deforming tool on the considered point of the soil layer based on the strength.

 doi:10.20944/preprints202605.0665.v1

The following expression will demonstrate the concentrated force P (N) through the resistance $R_{D.D.}$ (N), arising during the failure (deformation) of the soil monolith by the deforming tool into its individual components, H.

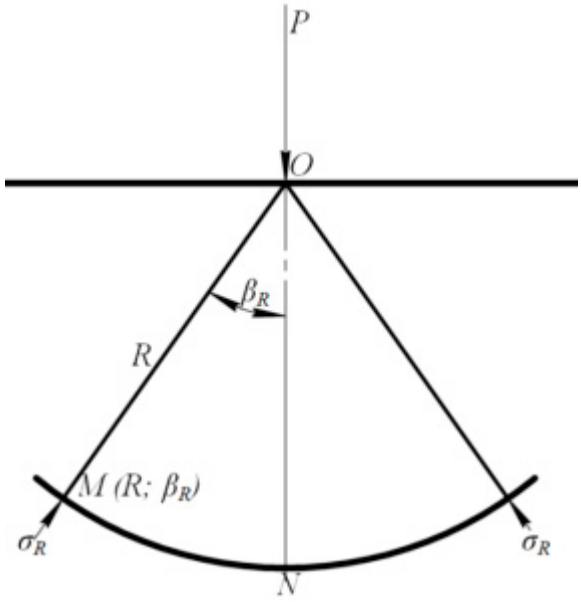

Figure 1. Diagram for determining the stress at the considered point M under the action of the concentrated force P.

To determine $R_{D.D.}$ (N), we make the following assumptions:

- stresses arising in the soil monolith as a result of the action of the deforming tool increase in proportion to the applied force;
- the velocity of the deforming tool is constant and equal to v (m/s), and the soil layer does not change its height during interaction with the tool, that is:

According to Figure 2, let us consider the deforming tool (dihedral wedge) with a working surface A_1BB_1, where $AA_1 = BB_1 = b_W$, $AB = A_1B_1 = l_W$. and the working surface AA_1BB_1 is inclined to the horizontal at a crushing angle α.

When the dihedral wedge transitions from position 1 to position 2, the force must be applied to it to overcome the deformation resistance exerted by the soil layer in the form of a resultant $R_{D.D.}$.

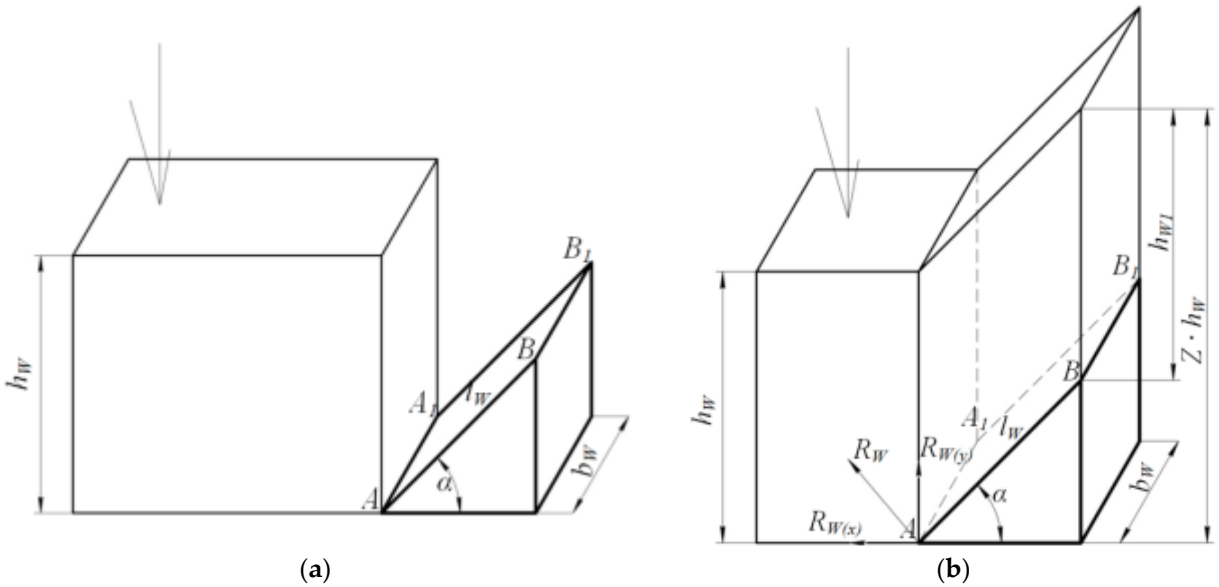

(**a**) (**b**)

Figure 2. Diagram of soil layer deformation by a two-faced wedge: (**a**) position 1; (**b**) position 2.

 doi:10.20944/preprints202605.0665.v1

Considering the adopted assumptions, the volume of the deformable soil layer $V_{D.S.}$ can be represented as follows:

$$V_{D.S.} = b_W \cdot h_W \cdot l_W \cdot cos\alpha. \quad (2)$$

The resultant force $R_{D.D.}$ can be resolved into horizontal $R_{D.D.(x)}$ and vertical $R_{D.D.(y)}$ components. The horizontal component $R_{D.D.(x)}$ represents the resistance exerted by the soil volume $V_{D.S.}$ against the penetration of the wedge AA_1BB_1:

$$R_{D.D.(x)} = V_{D.S.} \cdot k_{D(x)}, \quad (3)$$

where $k_{D(x)}$ is the horizontal component of the specific resistance of the soil to volumetric deformation, expressed in N/m³.

The vertical component $R_{D.D.(y)}$ – corresponds to the resistance offered by the soil volume $V_{D.S.}$ when its structural integrity is disrupted during vertical displacement. The change in height relative to the selected reference point (penetration depth of the deforming tool, h_W) is expressed using the dimensionless coefficient Z:

$$Z = \frac{h_W}{l_W \cdot sin\alpha}, \quad (4)$$

where l_W is the length of the working face of the dihedral wedge, m.

That is, relative to the bottom of the furrow located at the penetration depth of the deforming tool h_W, the volume of the deformable soil $V_{D.S.}$ will be raised by a factor of Z. Consequently, the expression for calculating the vertical component $R_{D.D.(y)}$ can be written as follows:

$$R_{D.D.(y)} = V_{D.S.} \cdot Z \cdot k_{D(y)}, \quad (5)$$

where $k_{D(y)}$ .is the vertical component of the specific resistance of the soil to volumetric deformation, in N/m³.

The product of the cosine of the angle α and the square root of the sum of the squares of $k_{D(x)}$ and $Z \cdot k_{D(y)}$ can be interpreted as the resultant specific resistance of the soil to volumetric deformation for the dihedral wedge with the crushing angle. Hence, following the vector addition rule, the resultant force $R_{D.D.}$ will be determined by the following formula:

$$R_{D.D.} = b_W \cdot h_W \cdot l_W \cdot k_{D(\alpha)}. \quad (6)$$

The validity of the presented equality is corroborated by the findings of various authors, as reported, for example, in [19–21,32], which conclude that the resultant specific resistance of the soil to volumetric deformation, k_D, is a function of the following variables: the crushing angle, the lifting height of the deformable soil layer, and the physico-mechanical properties of the soil.

The value $k_{D(\alpha)}$ was determined through tensometric measurements of dihedral wedges under field conditions on soils typical for the studied region followed by subsequent mathematical processing of the experimental data. The methodology for determining the specific resistance of soil to volumetric deformation is outlined in Section 2.2.Considering equation (6), formula (1) can be written as follows:

$$\sigma_R = \frac{3 \cdot b_W \cdot h_W \cdot l_W \cdot k_{D(\alpha)} \cdot cos\beta_R}{2 \cdot \pi \cdot R^2}. \quad (7)$$

Based on calculations according to formula (7), stress distribution diagrams were constructed for three distinct soil zones:

- Soil layer failure zone (distribution of ultimate stresses), where the condition $\sigma_R > \sigma_{LIMIT}$ is satisfied;
- High-deformation soil layer zone, where the condition $0.50 \cdot \sigma_{LIMIT} \leq \sigma_R < \sigma_{LIMIT}$ is satisfied;
- Soil layer partial-deformation zone, for which the condition $0.25 \cdot \sigma_{LIMIT} \leq \sigma_R < 0.50 \cdot \sigma_{LIMIT}$ is satisfied.

 doi:10.20944/preprints202605.0665.v1

Using the least squares method, a regression equation of the form y=f(x) was derived to approximate the curve delimiting the soil layer failure zone $S_{D.(F)}$ as well as the high- and partial-deformation zones $S_{D.(H.)}$ and $S_{D.(P.)}$.

Subsequently, the definite integral was applied to compute the corresponding areas$S_{D.(R)}$ and $S_{D.(H.)}$, and $S_{D.(P.)}$:

$$S_{D.(F)} = \int_{-x_F}^{x_F} f(x)_{(F)} dx_F, \quad (8)$$

$$S_{D.(H)} = \int_{-x_H}^{x_H} f(x)_{(H)} dx_H - \int_{-x_F}^{x_F} f(x)_{(F)} dx_F, \quad (9)$$

$$S_{D.(P)} = \int_{-x_P}^{x_P} f(x)_{(P)} dx_P - \int_{-x_H}^{x_H} f(x)_{(H)} dx_H - \int_{-x_F}^{x_F} f(x)_{(F)} dx_F, \quad (10)$$

where $f(x)_{(F)}$, $f(x)_{(H)}$ and $f(x)_{(P)}$ is a regression equation approximating the curves delimiting the areas of the soil layer failure zone $S_{D.(F)}$, the high-deformation zone $S_{D.(H)}$, and the partial-deformation zone $S_{D.(P)}$.

The total area of the deformable soil $S_{D.}$(m²) is then determined as the sum of the areas $S_{D.(F)}$, $S_{D.(H)}$ and $S_{D.(P)}$.

2.2. Methodology for the Experimental Determination of the Specific Resistance of Soil to Volumetric Deformation

In the initial phase of the research, strain gauging of variants of dihedral wedges mounted on the field unit was conducted. In the subsequent phase, mathematical processing of the obtained initial data was undertaken to ascertain the value of $k_{D(\alpha)}$for various angles α. The general view of the field unit and variants of dihedral wedges, and the stand for their fixation,is presented in Figure 3.

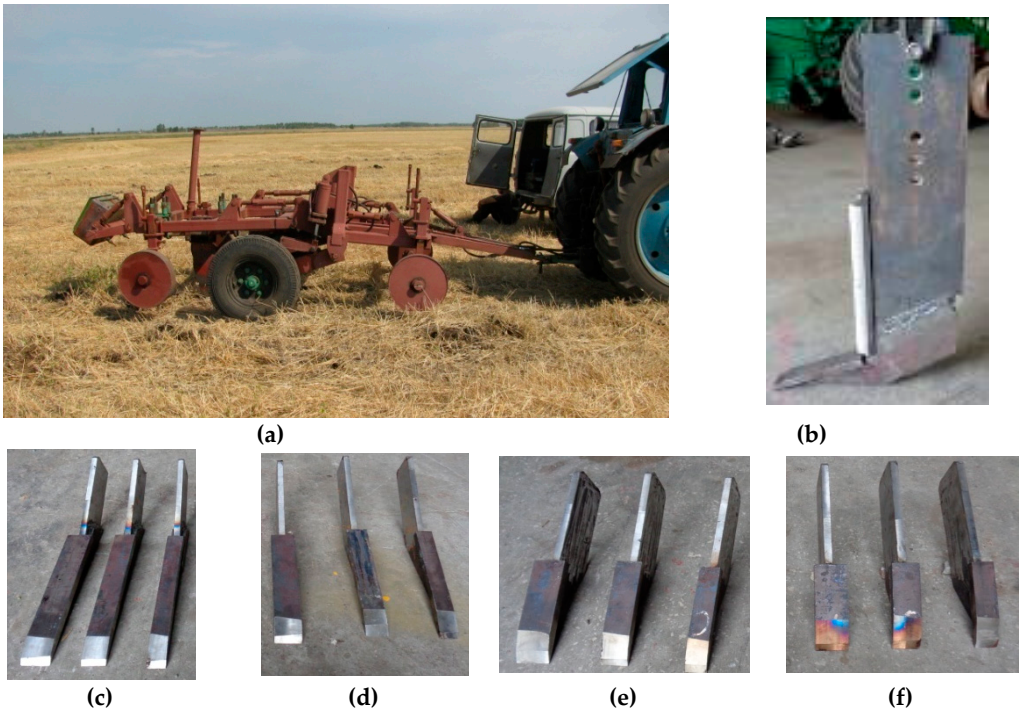

Figure 3. Field unit, variants of dihedral wedges, and stand for their fixation:**(a)** Field unit. General view; **(b)** Stand for fixation of dihedral wedge variants;**(c)** Dihedral wedges, α = 10°, b = 0.4–0.6 m;**(d)** Dihedral wedges, α = 20°, b = 0.4–0.6 m;**(e)** Dihedral wedges, α = 30°, b = 0.4–0.6 m; **(f)** Dihedral wedges, α = 40°, b = 0.4–0.6 m.

As illustrated in Figure 3, the field unit, in addition to the hitch, was equipped with4 support points (metal support wheels) located at each corner of the frame when in the working position. This

 doi:10.20944/preprints202605.0665.v1

structural configuration eliminatedthe unit's weight-related influence on draft resistance, which otherwise results fromfriction between the components of the working element and the soil.

The weight of the laboratory unit, excluding the working element, was determined to be G_e = 1900 N. The weight of a single working element was found to be G_(w.e) = 650 N. The rolling friction coefficient was established as f_c = 0.2.

A series of dihedral wedges were methodically affixed to the stand, which was then attached to the frame of the field unit. The wedges were then advanced through the soil at a depth of 0.3 m. During the movement of the field unit, the initial data were recorded. These included the resultant draft resistance of the field unit ($R_{F.I.}$, N) and the travel speed (V, m/s).

The resultant draft resistance was measured using strain-gauge equipment, which included a tensile force sensor (strain-gauge link) with a measurement range of up to 2.0 t (manufacturer: KB "SPC Agricultural engineering", Kazakhstan), plates for installing the strain-gauge link (manufacturer: KB "SPC Agricultural engineering", Kazakhstan), a ZET017-T8 strain-gauge station (manufacturer: ZETLAB, Russia), a portable personal computer Acer Aspire E 15 (manufacturer: Acer, China), a 12–220 V voltage converter Robiton R300 (manufacturer: Robiton, China), and connecting wires (see Figures 4 and 5).

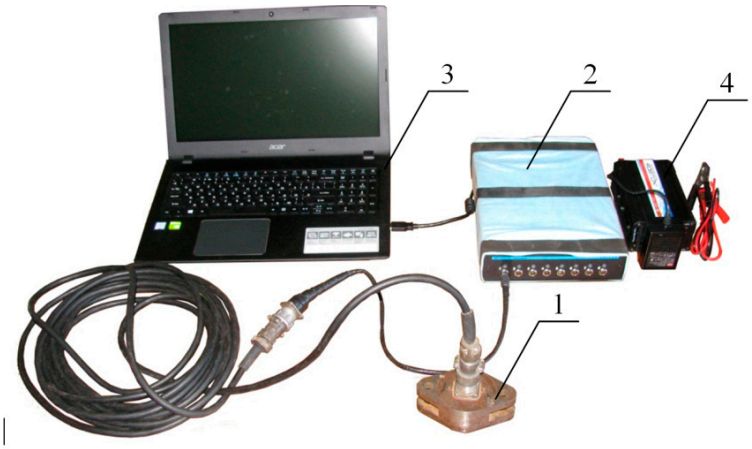

Figure 4. General view of the strain-gauge equipment: 1. Compression strain-gauge link (20 kN); 2. Strain-gauge station; 3. Portable PC; 4. 12–220 V voltage converter.

(a) **(b)**

Figure 5. Components of the strain-gauge equipment installed on the tractor's hitch system. **(a)** General view; **(b)** Mutual arrangement of the strain-gauge equipment components, the tractor hitch system, and the field unit. 1 — Strain-gauge link; 2 — Plate for mounting the strain-gauge link; 3 — Tractor hitch system; 4 — Laboratory unit.

The error of the strain-gauge measuring equipment, as determined in accordance with [33,34] specified, was found to be 1.96%. Geometric dimensions were measured using an R5 ICR tape measure, categorized as second-class in terms of accuracy.Mass characteristics were determined using tension dynamometers of the following models: DSI-0,1, DSI -0,5, and DSI -100. It is imperative

 doi:10.20944/preprints202605.0665.v1

to note that all measuring instruments are accompanied by a certificate of verification of the established type.

The test conditions were defined in accordance with GOST 20915-2011 [28].

The methodology for determining tillage depth is outlined in accordance with the provisions set out in GOST 33736-2016 [29], while the methodology for determining the resultant draft resistance of the field unit (N) and its travel speed (m/s) is outlined in accordance with GOST 34631 [30], respectively. The experiment was replicated on five occasions. The experimental research plan is presented in Table 1.

Table 1. Experimental Research Plan.

	Variable Parameters		
	***b*, m**	***α*, degree**	***V*, m/s**
	0.04-0.06 (step 0.01)	**10- 40 (step 10)**	**1.7-2.9 (step 0.3)**
Evaluated Parameter	$R_{F.I.}$, N		
Total number of experiments – 60, repetition: 5-fold			

The obtained initial data were used to determine the value of the specific resistance of soil to volumetric deformation:

$$k_{D(\alpha)} = \frac{R_{F.I.} - g \cdot f \cdot (m_{F.I.} + m_S + m_W) - b_W \cdot h_W \cdot \rho_S \cdot \left(g \cdot l_W \cdot \sqrt{1 + \frac{tg(\alpha+\varphi)}{\sin\alpha}}\right)}{b_W \cdot h_W \cdot l_W \cdot cos\alpha} + \frac{b_W \cdot h_W \cdot \rho_S \cdot \left(v^2 \cdot sin \propto \cdot \sqrt{1 + tg(\alpha+\varphi)}\right)}{b_W \cdot h_W \cdot l_W \cdot cos\alpha}. \quad (11)$$

where$g$ - acceleration due to gravity, m/s²;

f- rolling friction coefficient;

$m_{F.I.}$ - mass of the field unit, kg;

m_S - mass of the stand, kg;

$m_{W.}$ - mass of the dihedral wedge, kg;

ρ_S - soil density, kg/m³;

α - wedge installation angle relative to the furrow bottom (crushing angle), deg.;

φ - soil-on-steel friction angle, deg.

The specific resistance of the soil to volumetric deformation for a wedge with an angle of α was determined by adopting the arithmetic mean value. In order to assess the homogeneity and stability of the obtained set of values for the specific soil resistance, the coefficient of variation, $\boldsymbol{\upsilon}$, was utilised. The methodology for determining the relevant sources is outlined in [35] and is to be followed.

3. Findings

3.1. The Following Report Summarises the Findings of an Experimental Study Undertaken to Ascertain the Specific Resistance of Soil to Volumetric Deformation

The values of $k_{D(\alpha)}$ for various angles α are presented in Table 2

Table 2. Values $\mathbf{k_{D(\alpha)}}$ for deforming tools with different angle $\boldsymbol{\alpha}$.

Angle α, degrees	10	20	30	40
Specific soil resistance to volumetric deformation $k_{D(\alpha)}$, N/m³	$7.00 \cdot 10^5$	$6.49 \cdot 10^5$	$7.66 \cdot 10^5$	$8.01 \cdot 10^5$

 doi:10.20944/preprints202605.0665.v1

The soil hardness in the 30-centimetre layer was found to be 7.1 MPa, with a moisture content of 17.6% and a density of 1330 kg/m³. These conditions are considered typical for the region under consideration during fall plowing.

It was established that changes in travel speed within the considered speed range did not affect the value of $k_{D(\alpha)}$. The set of values obtained for specific soil resistance was homogeneous and stable. The coefficient of variation is thus υ=6.5%.

The values of $k_{D(\alpha)}$ presented in Table 2 were utilised in the mathematical modelling of soil layer deformation processes by tillage working elements, which are based on the dihedral wedge, under the conditions of the northern region of Kazakhstan.)

3.2. Findings of Stress Determination in the Soil Layer Under the Action of a Dihedral Wedge

According to the developed research methodology, the relationship was established between the area of the deformable soil zone $S_{D.}$ (m²) and the length of the dihedral wedge l_W(m). The length of the dihedral wedge varied within the range l_W = [0.05; 0.30] m, while its width remained constant at b_W = 0.06 m. The installation angle of the dihedral wedge relative to the furrow bottom was α = 20°.

Calculations performed using formulas (7)–(10) produced the following results:

- Stress distribution profiles in the soil layer for various lengths of the dihedral wedge are presented in Figure 6;
- The functional relationship $S_{D.} = f(l_W)$ is shown in Figure 7.

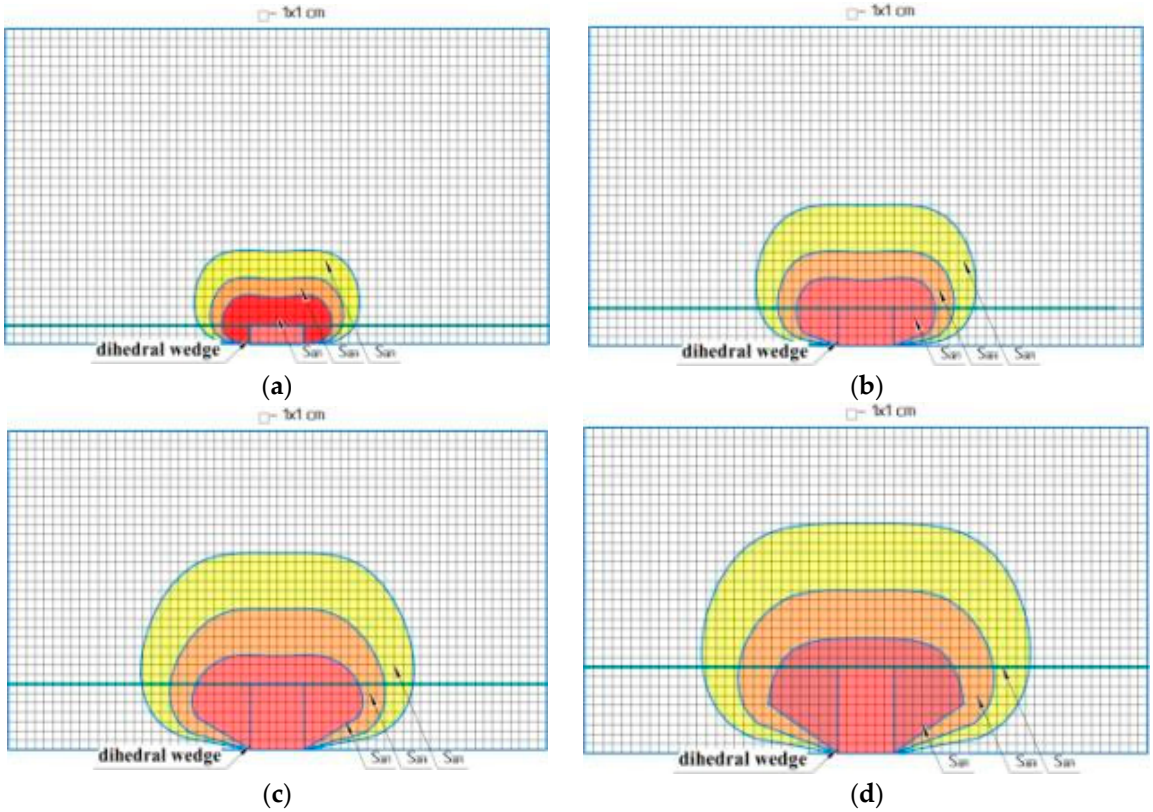

 doi:10.20944/preprints202605.0665.v1

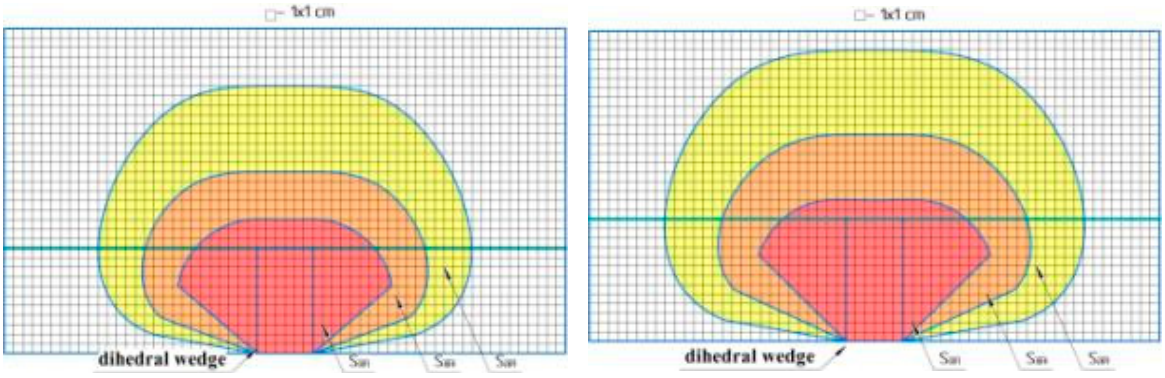

(**e**) (**f**)

Figure 6. Stress distribution diagrams in the transverse-vertical plane for dihedral wedges of varying lengths l_W: (**a**) l_W = 0.05 m; (**b**) l_W = 0.10 m; (**c**) l_W = 0.15 m; (**d**) l_W = 0.20 m; (**e**) l_W = 0.25 m; (**f**) l_W = 0.30 m.

As shown in Figure 4, increasing the length of the dihedral wedge from 5 to 30 mm corresponding to an 83% relative increase leads to an expansion of the deformable soil zone (S_D, m²) from 0.02 to 0.10 m², representing an 80% growth. This demonstrates that the area of the deformable soil increases approximately proportionally to the length of the dihedral wedge.

The identified quantitative relationship between the dihedral wedge length (l_W, m) and the area of the deformable soil zone (S_D, m²) can be utilized in the design of soil-engaging implements. Specifically, it can inform the determination of the projection of a flat-cutting working element during the theoretical design and analysis phase.

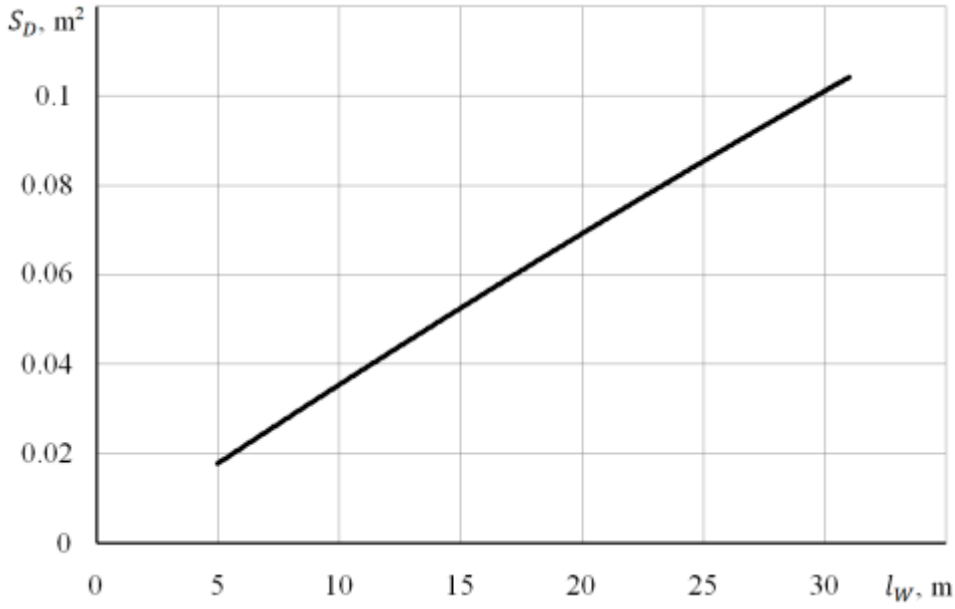

Figure 7. Influence of the dihedral wedge length (l_W, m) on the total area of the deformable soil (S_D, m²).

The relationship between the length of the dihedral wedge and the area of deformed soil was identified and used to substantiate the parameters of the flat-cutting working element for processing soils with a heavy physical and mechanical composition and low moisture content in geographical regions prone to wind erosion. One of the most common methods of reducing the risk of wind erosion is to maintain a protective layer of stubble and crop residues on the field surface. In the context of the prevailing soil and climatic conditions, implementation of flat-cutting working elements is deemed the most efficacious approach in ensuring adherence to agrotechnical requirements.

It is hypothesised that the percentage of preserved stubble can be increased after soil treatment with flat-cutting working elements, and that a sufficient level of soil crumbling can be maintained by

 doi:10.20944/preprints202605.0665.v1

increasing the working width of the flat-cutting element and simultaneously increasing the length of the share (namely, its cantilever part).

In order to facilitate a quantitative assessment of the quality of soil crumbling at the theoretical research stage, a soil layer deformation interference coefficient was proposed. This was determined by the following formula::

$$\lambda_I = \frac{S_D}{S_{FC}} = \frac{S_D}{B_{FC} \cdot h_W}, \quad (12)$$

whereλ_I – soil layer deformation interference coefficient;

S_{FC} – total area of soil processed by the flat-cutting working element, m²;

B_{FC} – working width of the flat-cutting working element, m.

The following physical interpretation can be deduced from the formula. The flat-cutting working element primarily affects the soil layer with its share and moldboards. As the cutting edge of the share is offset forward relative to the cutting edges of the moldboards, it is the share that exerts the initial impact on the soil monolith (see Figure 8a).

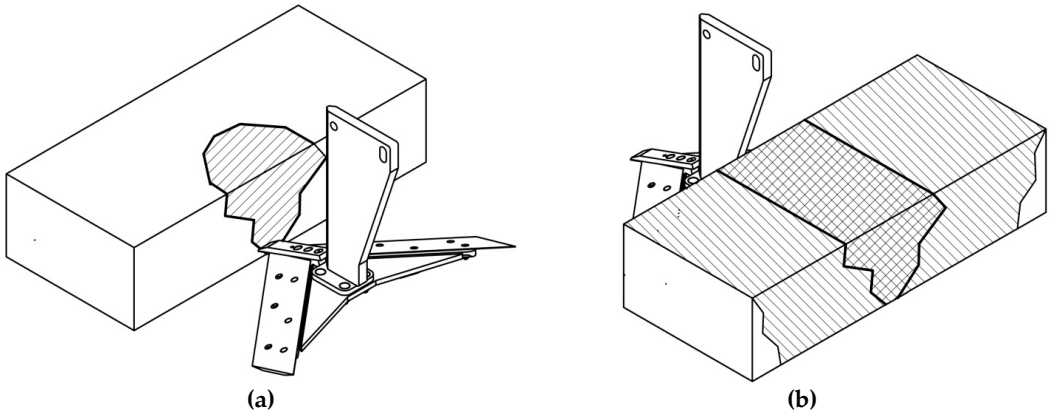

(a) **(b)**

Figure 8. Interaction process of the flat-cutting working element components with the soil monolith cross-section: **(a)** interaction of the share**; (b)** interaction of the moldboards.

In accordance with the research findings presented in Section 2.1, the following conclusions can be drawn: under the influence of the phenomenon under investigation, zones of soil layer destruction are formed, zones of increased deformation $S_{D.(R)}$ and $S_{D.(H.)}$, and $S_{D.(P.)}$ respectively. At the moment of contact between the cutting edge of the moldboards and the considered cross-section of the soil layer (see Figure 8, b), an interaction (interference) of the trajectories of the shear lines, caused by the moldboards, with the already existing cracked section in the soil will occur. Consequently, the intensity of soil crumbling in this area will be at its greatest. The location of this zone is to be determined in the central part of the working element, with respect to the longitudinal-vertical plane that passes through the axis of symmetry of the flat-cutting working element. In the peripheral region of the flat-cutting working element situated beyond the soil deformation interference zone the onset of fractures in the soil will be predominantly triggered by the impact of the moldboard cutting edges on the soil monolith. However, this is insufficient for the intensive progression of the cracking process when working with soils of a heavy physical-mechanical composition and low moisture. Consequently, an increase in the value of $\lambda_I$will result in greater levels of soil crumbling.

In the context of the flat-cutting working element, implementation of the technological operation under consideration is deemed to be satisfactory provided that the soil is crushed to a level of 60–65% (provided that the stubble retention is no less than 60%). It has been established that the specified crushing value corresponds to $\lambda_I = 0.18$. This value was adopted as the reference standard.

A correlation was identified between the working width of the flat-cutting element and the length of the chisel cantilevered part, which ensured increased stubble retention and an adequate level of soil crushing. The calculation results are presented in Figure 9.

 doi:10.20944/preprints202605.0665.v1

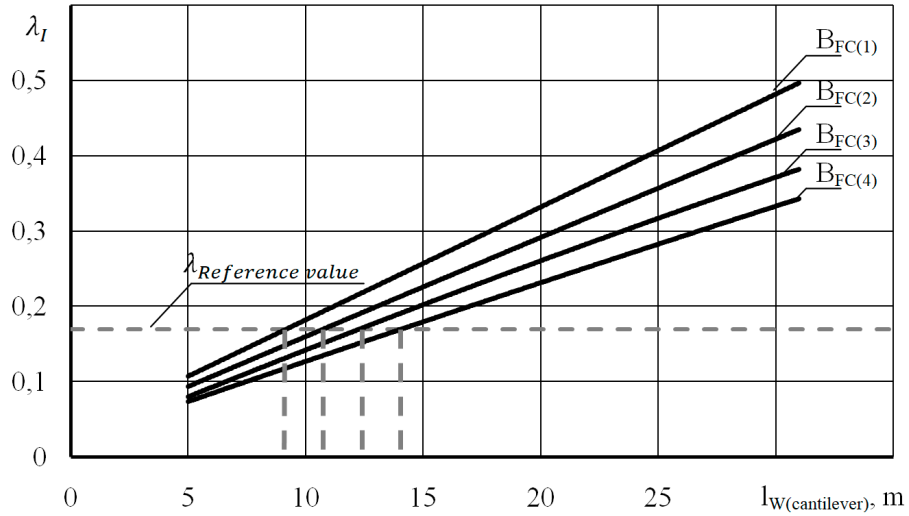

Figure 9. Influence of the length of the chisel cantilevered part $l_{W(cantilever)}$ (m) and the working width of the flat-cutting working element B_{FC} (m) on the soil layer deformation interference coefficientλ_I: $B_{FC(1)}$ = 0.7 m; $B_{FC(2)}$ = 0.8 m; $B_{FC(3)}$ = 0.9 m; $B_{FC(4)}$ = 1.0 m.

As demonstrated in Figure 9, an increase in the working width of the flat-cutting working element requires a corresponding increase in chisel length to ensure the required level of soil crushing, expressed through the interference coefficient λ_I. It is therefore evident that, contingent upon the working width of the flat-cutting working element, the condition for the requisite crushing is fulfilled at the following values:

- atB_{FC}= 0,7 m$l_{W(cantilever)}$ ≥ 8.0 mm;
- atB_{FC}= 0,8 m$l_{W(cantilever)}$ ≥ 11.0 mm;
- tB_{FC}=0,9 m$l_{W(cantilever)}$ ≥ 14.0 mm;
- atB_{FC}=1,0 m$l_{W(caantilever)}$ ≥ 17.0 mm.

The $B_{FC(1)}$ - $B_{FC(4)}$ curves do not exhibit an optimum zone; therefore, it was not possible to draw an unambiguous conclusion regarding the optimal width of the flat-cutting working element and the length of the chisel cantilevered part at this stage of the research. It is imperative to consider the influence of the analyzed design parameters on the energy performance. An unwarranted increase in the chisel length not only raises the interference coefficient value, thereby intensifying soil crushing, but also leads to higher draft resistance of the flat-cutting working element in comparison. This, in turn, will have a detrimental effect on the energy intensity of the technological process under consideration.

The manufactured variants of the flat-cutting working elements are presented in Figure 10.

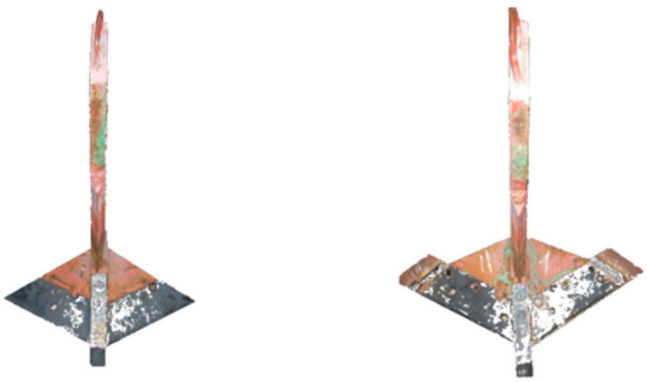

(a) **(b)**

 doi:10.20944/preprints202605.0665.v1

(c) (d)

Figure 10. Optionsofflat-cuttingworkingelementsmanufacturedforexperimentalresearch: **(a)**B_{FC}= 0.6 m; **(b)**B_{FC}= 0.7 m; **(c)**B_{FC}= 0.8 m; **(d)**B_{FC}= 0.9 m.

The manufactured options of chisels with different lengths are presented in Figure 11.

As this article is dedicated to the description of the method developed by us for determining stresses in the soil layer under the influence of the dihedral wedge, it is not possible to present here the comprehensive research findings on substantiating the optimal working width and chisel length of the flat-cutting working element. The research results substantiating the said parameters of the flat-cutting working elements will be presented in more detail in future publications.

For example, the mathematical model we developed was used to justify the projection of the chisel in variants of flat-cutting working tools for deep tillage of compacted soils [36], as well as in the flat-cutting working tool of the cultivator-fertilizer for subsurface application of mineral fertilizers [37]. Photographs of these working tools are presented in Figure 5.

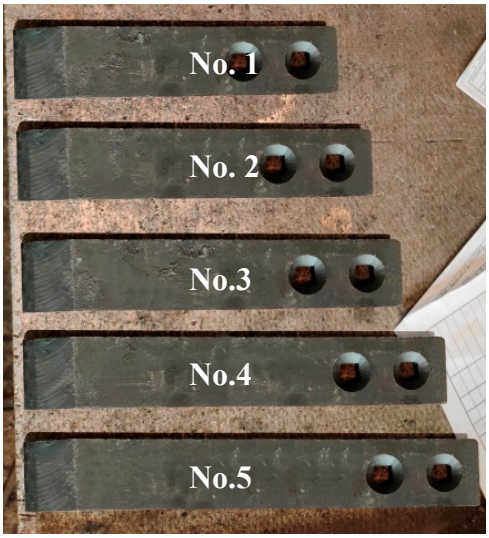

Figure 11. Chisel options manufactured for experimental research are as follows: option No. 1 (standard chisel) l_W = 285 mm, $l_{W(cantilever)}$ = 50 mm; option No. 2 l_W = 315 mm, $l_{W(cantilever)}$ = 80 mm; option No. 3 l_W = 345 mm, $l_{W(cantilever)}$ = 110 mm; option No. 4 l_W = 375 mm, $l_{W(cantilever)}$ = 140 mm; option No. 5 l_W = 405 mm, $l_{W(cantilever)}$ = 170 mm.

 doi:10.20944/preprints202605.0665.v1

(**a**) (**b**) (**c**)

Figure 12. Variants of flat-cutting working tools with substantiated chisel projection: (**a**) for soil tillage to a depth of 20-35 cm (working tool width 0.6 m, chisel projection 5 cm); (**b**) for soil tillage to a depth of 20-35 cm (working tool width 0.7 m, chisel projection 8 cm);(**c**) for soil tillage to a depth of 14-25 cm (working tool width 0.7 m, chisel projection 8 cm).

4. Discussion

The development of the graphical-analytical method for determining the stresses induced in a soil layer by the dihedral wedge was based on an equation proposed by J. Boussinesq. This method incorporates the effects of both the wedge parameters and the physical-mechanical properties of the soil. The findings of the study demonstrated the direct proportional relationship between the length of the dihedral wedge and the total area of the deformable soil. Specifically, an 83% increase in wedge length (from 0.05 to 0.30 m) resulted in an 80% increase in the area of deformable soil (from 0.02 to 0.10 m²).

The proposed graphical-analytical method has the potential to be applied in the design of soil-engaging implements. For instance, it can be used to justify the projection of a flat-cutting working element during the theoretical research and design stage.

Author Contributions: Conceptualization, A.K., A.D. and I.V.; methodology, A.K. and Y.P.; software, I.T.; validation, A.K., P.I and A.S.; investigation, A.K., A.D., I.T..; data curation, P.I.; A.S.; writing—original draft preparation, A.K. and A.D.; writing—review and editing, Y.B. and Y.P. ; visualization, I.T.; supervision, A.K.; funding acquisition, Y.B. All authors have read and agreed to the published version of the manuscript.

Funding: This research was funded by the Industrial Development Committee of Industry of the Ministry of Industry and Construction of the Republic of Kazakhstan (Grant №. BR23992300).

Data Availability Statement: All data used in this study are publicly accessible at the following link: https://doi.org/10.5281/zenodo.18884094.

Conflicts of Interest: The authors declare no conflicts of interest.

References

1. Lamande M., Schjonning P. Soil mechanical stresses in high wheel load agricultural field traffic: a case study. *Soil research*,**2017**,*56(2)*, 129-135. doi: 10.1071/SR17117.
2. Hamza M.A.., Anderson W.K. Soil compaction in cropping systems: A review of the nature, causes and possible solutions. *Soil and tillage research*,**2005**, *82(2)*, 121-145. doi:10.1016/j.still.2004.08.009.
3. Yang P., Dong W., Heinen M., Qin W., Oenema O. Soil compaction prevention, amelioration and alleviation measures are effective in mechanized and smallholder agriculture: a meta-analysis. *Land*,**2022**, 11, 645. doi:10.3390/land11050645.

 doi:10.20944/preprints202605.0665.v1

4. Schjonning P., Lamande M., Thorse M. *Soil compaction – drivers, pressures, state, impacts and responses*. Danish Centre for Food and Agriculture: Tjele, Denmark,**2019**, 34 p.
5. 1-8Chamen T., Moxey A.P., Towers W., Balana B., Halett P.D. Mitigating arable soil compaction: A review and analysis of available cost and benefit data. *Soil and tillage research*,**2015**, 146, 10-25. doi:10.1016/j.still.2014.09.011.
6. Bondarev A.G., Puponin A.I., Matyuk N.S. *Over-compaction of arable soils: causes, consequences, ways of reduction*. Nauka: Moscow, USSR, **1987**, 215 p.
7. Mudarisov S., Gainullin I., Gabitov I., Hasanov E., R., Farhutdinov I. Soil compaction management: reduce soil compaction using a chain-track tractor. *Journal of terramechanics*, **2020**, 89, 1-12. doi: 10.1016/j.jterra.2020.02.002.
8. El-Sayegh Z., El-Gindy M., Johansson I., Oijer F. Improved tire-soil interaction model using FEA-SPH simulation. *Journal of terramechanics*, **2018**, 78, 53-62. doi:10.1016/j.jterra.2018.05.001.
9. Antille D.L., Peets S., Galambosova J., Botta G.F., Rataj V., Macak M., Tullberg J.N. Review: Soil compaction and controlled traffic farming inarable and grass cropping systems. *Agronomy research*, **2019**, 17(3), 653-682. doi: 10.15159/AR.19.133.
10. Pholpho T., Pholpho K. Multi - role hovercraft for agricultural. In Proceedings of the12th TSAE International Conference. IOP Conf. Series: Earth and Environmental Science, IOP Publishing: Chonburi, Thailand, 14-15 March 2019.doi: doi:10.1088/1755-1315/301/1/012013.
11. Nair A., Pai K., Varghese M., Thomas S. Hovercraft based farming system. *International Journal of Science and Research (IJSR)*, **2014**, 2(1), 17-22.
12. Beloev H. Methodology for experimental study of soil microrelief on ruts in bridge farming. *Machinery and Energetics*, **2022,** 13(4). doi: 10.31548/machenergy.13(4).2022.9-15.
13. Chamen T., Controlled traffic farming – from worldwide research to adoption in europe and its future prospects. *Acta TechnologicaAgriculturae*, **2015**, 3, 64-73. doi: 10.1515/ata-2015-0014.
14. Peixoto D., Moreira da silva L., Batista de Melo L., et al. Occasional tillage in no-tillagee systems: a global meta-analysis. *Scince of the total environment*,**2020**, *745*, 140887. doi: 10.1016/j.scitotenv.2020.140887.
15. Peralta G., Alvarez C., Taboada M. Soil compaction alleviation by deep non-inversion tillage and crop yield responses in no tilled soils of the Pampas region of Argentina. A meta-analysis. *Soil and tillage research*,**2021,***211*, 105022. doi: 10.1016/j.still.2021.105022.
16. Qaisrani R., Jianqiao L. Application of Bio-Inspired Surfaces in Reducing Adhesion to the Surfaces of Soil-Engaging Components of Agricultural and Earth-Moving Machinery. In *Bio-Inspired Surfaces and Applications*.Ng E.Y.K., Luo Y. World Scientific Publishing Co: New Jersey, USA, **2016**, pp. 485-553.
17. Balovnev V.I. *Road-building machines with working or gans of intensifyingaction*. Mashinostroenie: Moscow, USSR, **1981**, 224 p.
18. *The system of criteria for quality, reliability, and economic efficiency of agricultural machinery: an instructional and methodological publication*, Rosinformagrotekh: Moscow, Russia,**2010**, 310 p.
19. Sineokov G.N. *Design of the tillage implement*, Mashinostroenie: Moscow, USSR,**1965**, 310 p.
20. Vagin A.T. Larchenkov L.V. Piletskiy A.Z. *Mechanization of soil protection from wind erosion in the Non-Chernozem zone*, Kolos: Leningrad, USSR.**1977**, 272 p.
21. Panov I.M.. Vetokhin V.I. *Physical foundations of soil mechanics*, Feniks: Kyev, Ukraine**, 2008**. 265 p.
22. Mudarisov S., Lobachevsky Y., Farkhutdinov I. Justification of the soil dem-model parameters for predicting the plow body resistance forcec during plowing. *Journal of terramechanics*,**2023**,*109*,37-44. doi: 10.1016/j.jterra.2023.06.001.
23. Hoseinian S., Hemmat A., Esehaghbeygi A. Development of a dual sideway-share subsurface tillage implement: Part 1. Modeling tool interaction with soil using DEM. *Soil and tillage research*. **2022**,*215*. doi: 10.1016/j.still.2021.105201.
24. Lima R., Keller T. Soil stress measurement by load cell probes as influenced by probe design, probe position, and soilmechanical behavior. *Soil and tillage research*, **2021**,*205*. doi: 10.1016/j.still.2020.104796.
25. Sun J., Wang Y., Ma Y. DEM simulation of bionic subsoilers (tillage depth >40 cm) with drag reduction and lower soil disturbance characteristics. *Advances in engineering software*. **2018**, *119*, 30-37. doi: 10.1016/j.advengsoft.2018.02.001.

 doi:10.20944/preprints202605.0665.v1

26. Tsypuk A.M. Justification of the size of the stress region in the soil under the influence of mechanical load. *Trudy lesoinzhenernogofakultetaPetrGU*,**1999**; 172-174.
27. Ibarra S., McKyes E., Broughton R. A model of stress distribution and cracking in cohesive soils produced by simple tillage implements. *Journal of terramechanic*,**2005**, *42(2)*, 115-139. doi: 10.1016/j.jterra.2004.08.002.
28. GOST 20915-2011. *Testing of agricultural tractors and machines. Procedure for determination of test conditions*, Standartinform: Moscow, Russia, **2013**, 27 p.
29. GOST 33736-2016. *Agricultural machinery. Machines for deep tillage. Test methods*, Standartinform: Moscow, Russia, **2017**, 39 p.
30. GOST 34631-2019. *Agricultural machinery. Methods of power estimation*, Standartinform: Moscow, Russia, **2020**, 13 p.
31. Vaghela, K. *Principles and Practices of Soil Mechanics and Foundation Engineering*. Marcel Dekker: New York, USA, **2008**, 1050 p.
32. Burchenko P.N. *Mechanical and technological foundations of new generation tillage machines*. VIM:Moscow, **2002**, 212 p.
33. Montero W., Farag R., Diaz V., Ramirez M., Boada B.L., Uncertainties associated with strain-measuring systems using resistance strain gauges. The Journal of Strain Analysis for Engineering Design, 2011, 1(46), 1-13. doi: 10.1243/03093247JSA661
34. Sujatha C. Strain Gauge-Based Equipment. In *Vibration, Acoustics and Strain Measurement*. Sujatha C. Springer, Cham, Switzerland, **2023**, pp. 305-349.doi: 10.1007/978-3-031-03968-3_7
35. Stepniak C. Coefficient of variation. In *International encyclopedia of statistical science*. Lovric M. Springer, Cham, Switzerland, **2025**, pp. 305-349. doi: doi.org/10.1007/978-3-662-69359-9_117
36. Kuvaev A., Derepaskin A., Tokarev I. Substantiation of the working width of the tillage implement. *Acta Universitatis Agriculturae et SilviculturaeMendelianae Brunensis*. **2021**,*69(1)*, 21-31. doi: 10.11118/actaun.2021.002.
37. Kuvaev A., Derepaskin A., Tokarev I., Polichshuk Y., Binyukov Y., Ivanchenko P., Kukhar V., Semibalamut A. Optimizing cultivator-fertilizer performance with tractor-mounted configuration in northern Kazakhstan. *International journal of agriculture and biosciences*.**2025**,*14(4)*, 674-682. doi: 10.47278/journal.ijab/2025.076.